Hindawi
Journal of Nanomaterials
Volume 2018, Article ID 7619419, 15 pages
https://doi.org/10.1155/2018/7619419

Research Article

Electrochemical Determination of Paracetamol Using Fe_3O_4/Reduced Graphene-Oxide-Based Electrode

Nguyen Thi Anh Thu,[1] Hoang Van Duc,[1] Nguyen Hai Phong,[2] Nguyen Duc Cuong,[3] Nguyen Thi Vuong Hoan,[4] and Dinh Quang Khieu[2]

[1] *University of Education, Hue University, Hue 530000, Vietnam*
[2] *University of Sciences, Hue University, Hue 530000, Vietnam*
[3] *Faculty of Tourism and Hospitality, Hue University, Hue 530000, Vietnam*
[4] *Department of Chemistry, Quy Nhon University, Quy Nhon 590000, Vietnam*

Correspondence should be addressed to Dinh Quang Khieu; dqkhieu@hueuni.edu.vn

Received 8 November 2017; Revised 8 February 2018; Accepted 7 March 2018; Published 17 April 2018

Academic Editor: Zoraida González

The synthesis of magnetic iron oxide/reduced graphene oxide (Fe_3O_4/rGO) and its application to the electrochemical determination of paracetamol using Fe_3O_4/rGO modified electrode were demonstrated. The obtained materials were characterized by means of X-ray diffraction (XRD), nitrogen adsorption/desorption isotherms, X-ray photoelectron spectroscopy (XPS), transmission electron microscope (TEM), Fourier transform infrared spectroscopy (FTIR), and magnetic measurement. The results showed that Fe_3O_4/rGO composite exhibited high specific surface area, and its morphology consists of very fine spherical particles of Fe_3O_4 in nanoscales. Fe_3O_4/rGO was used as an electrode modifier for the determination of paracetamol by differential pulse-anodic stripping voltammetry (DP-ASV). The preparation of Fe_3O_4/rGO-based electrode and some factors affecting voltammetric responses were investigated. The results showed that Fe_3O_4/rGO is a potential electrode modifier for paracetamol detection by DP-ASV with a low limit of detection. The interfering effect of uric acid, ascorbic acid, and dopamine on the current response of paracetamol has been reported. The repeatability, reproducibility, linear range, and limit of detection were also addressed. The proposed method could be applied to the real samples with satisfactory results.

1. Introduction

Paracetamol (N-acetyl-*p*-aminophenol, acetaminophen) (henceforth PRC) is widely used as an active ingredient in pharmaceutical preparations as it is not considered to be carcinogenic at therapeutic doses [1]. PRC is available in different dosage forms: tablets, capsules, drops, elixirs, and suspensions [2]. A limited use of PRC does not cause any harmful side effects. However, overdosing and the chronic use of PRC produce toxic metabolite accumulation that will cause kidney and liver damage [1, 3]. Therefore, a sensitive, accurate, fast, and simple analytical method for estimating PRC in pharmaceutical preparations and human plasma is needed.

Numerous methods have been employed for detecting PRC, alone and in mixtures, in biological samples and formulations, such as HPLC (high-performance liquid chromatography) [4, 5], liquid chromatography-mass spectrometry (LC-MS) [2, 6, 7], spectrofluorimetry [8], electrochemical techniques [9, 10], chemiluminescence [11, 12]. However, these methods suffer from several disadvantages such as being time-consuming, high cost, and a requirement for sample pretreatment. In some cases, low sensitivity and selectivity limited their application. Anodic stripping voltammetric techniques (ASV) have been recognized as effective techniques for inorganic and organic compounds analysis because of numerous advantages such as faster analysis, higher selectivity and sensitivity, low cost, low detection limit, and a possibility of performing analysis in situ [13, 14]. Differential pulse-anodic stripping voltammetry (DP-ASV), considered as one kind of ASV methods, has been used for estimating several organic compounds because of its

remarkably high sensitivity. Glassy carbon electrodes chemically modified with porous materials such as mesoporous materials [15] and metal organic frameworks (MOFs) [16] have received considerable attention for ASV because they present significant improvements in terms of fast response, high selectivity, low detection limit, and renewability. The DP-ASV method has been widely employed to detect PRC in pharmaceutical preparations. The porous-material-modified electrodes, for instance, graphene-based electrodes [17], multiwalled carbon nanotube modified basal plane pyrolytic graphite electrode [18], and nanoparticles bismuth oxide modified glassy carbon electrode (GCE) [19], have been often used for electrochemical studies of PRC because of their unique properties such as high surface areas and many active sites.

Superparamagnetic iron oxides nanoparticles (NPs) hold a lot of promise for applications in electrochemical fields because of the unusual structure, excellent adsorption, catalytic properties, and inherent electrical conductivity [9, 20]. Reduced graphene oxide (rGO) is an important product of reducing graphene oxide (GO) or graphite oxide (GrO) using strong reductants such as hydrazine [21] and $NaBH_4$ [22], through high-temperature treatment [23], UV-assisted photocatalysis [24], or low-temperature annealing reduction [25, 26]. GO prepared from graphite by means of strong oxidizers [27] to form graphite oxide (GrO), followed by dispersing the resulting GrO in an appropriate solution for exfoliating into few layers, is well-known as a modified Hummers' method [27]. GrO or GO contains myriad oxide functionalities (predominantly alcohols and epoxides) but retains a stacked structure similar to graphite. However, rGO is rather different from GrO or GO in terms of structure. The rGO is exfoliated into monolayers or few-layered stacks. The surface functionality (particularly in basic media) greatly weakens the layer-layer interactions, due to its hydrophilicity [28]. rGO has received tremendous attention because of its high electrical conductivity, active surface, large surface area per volume, and excellent electrocatalytic properties [29, 30]. rGO can act as an excellent performance carrier, while NPs can be highly dispersed on its surface, and the charge transfer at the interface of these hybrid materials can provide a synergistic effect to bring about properties that are different from those of each individual component. Then, Fe_3O_4/rGO composites provide a potential application in electrochemistry [9]. With the advantages of the magnetism and the conductivity of the Fe_3O_4/rGO composites, the nanocomposites could be easily adhered to the electrode surface to achieve the direct redox reactions and electrocatalytic behaviors of analytes adsorbed on the modified surface. In fact, Fe_3O_4/rGO was employed to produce FePc@Fe_3O_4/reduced graphene oxide nanocomposites as biomimetic catalysts for organic peroxide sensing [31], to modify GCE to design a high-performance electrochemical biosensing platform [32], and to load on the magnetic glassy carbon electrode (MGCE) to form a biosensor to test glucose [9]. To the best of our knowledge, there is no report based on using Fe_3O_4/rGO modified electrodes for the determination of PRC.

In the present paper, magnetic Fe_3O_4/rGO composite was prepared by a facile solvothermal method. The obtained Fe_3O_4/rGO was used as an electrode modifier to prepare a Fe_3O_4 graphene-modified glassy carbon electrode (Fe_3O_4/rGO/GCE), which can be used for sensitive detection of PRC in pharmaceutical products with the DP-ASV method.

2. Experimental

2.1. Materials. Graphite powder, potassium permanganate ($KMnO_4$), iron (II) chloride tetrahydrate ($FeCl_2{\cdot}4H_2O$), sodium acetate ($NaCH_3COO$), sodium citrate ($Na_3C_6H_5O_7$), sodium dihydrogen phosphate (NaH_2PO_4), sodium hydrogen phosphate (Na_2HPO_4), acetic acid (CH_3COOH), ascorbic acid ($C_6H_8O_6$), citric acid ($C_6H_8O_7$), boric acid (H_3BO_3), ammonia solution (NH_4OH, 25%), Nafion ($C_7HF_{13}O_5S{\cdot}C_2F_4$, 5%), hexamethylene tetramine (urotropine) ($(CH_2)_6N_4$), and paracetamol ($C_8H_9NO_2$) were purchased from Merck Company (Germany). Sodium nitrate ($NaNO_3$), ethanol (C_2H_5OH), hydroperoxide (H_2O_2, 30%), and potassium hydroxide (KOH) were supplied by Daejung Company (Korea). Phosphate buffer solution (PBS) pH 6 was prepared from 1 M NaH_2PO_4 and 1 M Na_2HPO_4. Citrate buffer solution (CBS) pH 6 was prepared from 1 M $Na_3C_6H_5O_7$ and 1 M $C_6H_8O_7$. Acetate buffer solution (ABS) pH 6 was prepared from 1 M CH_3COOH and 1 M $NaCH_3COO$. Urotropine buffer solution (UBS) pH 6 was prepared from 1 M $(CH_2)_6N_4$. pH 6 of buffers was adjusted with 1 M KOH or 1 M HCl. Britton–Robinson buffer solutions (B-RBS) in the range of pH from 4.8 to 9.8 were prepared from 0.5 M H_3BO_3, 0.5 M H_3PO_4, and 0.5 M CH_3COOH. The desired pH 6 of buffer was adjusted with 1 M KOH or 1 M HCl.

2.2. Methods. X-ray diffraction measurement was recorded on a Bruker D8-Advance X-ray diffractometer (Germany) with CuK_α radiation (λ = 0.1514 nm). Morphology was observed by means of transmission electron microscopy (TEM) using TEM Jeol JEM-2100F (Japan). FTIR analyses were conducted with a Nicolet Nexus 470 FTIR spectrometer (Thermo Nicolet, USA). X-ray photoelectron spectroscopy (XPS) was studied using a Shimadzu Kratos AXISULTRA DLD spectrometer. Peak fitting was conducted by means of the CASA XPS software. The analysis of iron element was conducted by atomic absorption spectrometry (AAS) using AA6800 Shimadzu (Japan). A CPA-HH5 Computerized Polarography Analyzer (Vietnam) was used for voltammetry experiments. All measurements were performed in the cell with three electrodes: a GCE with a diameter of 2.8 ± 0.1 mm used for formatting the modified electrode as working electrode, an Ag/AgCl/3M KCl as a reference electrode, and a platinum wire as an auxiliary electrode. All measurements were carried out at ambient temperature.

The HPLC (high-performance liquid chromatography) method was utilized to analyze PRC for the sake of comparison. Chromatographic determinations were performed in a Shimadzu 2030 HPLC system. The chromatographic conditions were HiQ sil C18 (250 mm × 4.6 mm), detector wavelength 225 nm, (water : methanol : acetic acid = 69 : 28 : 3) and mobile phase at ambient temperature.

2.3. Synthesis of GO, rGO, and Fe_3O_4/rGO. Graphite oxide (GrO) was prepared using the Hummers method [27] according to our previous paper [33]. For the synthesis of rGO, the as-prepared GrO (0.1 g) was exfoliated by ultrasonication in 100 mL of distilled water for 1 h to prepare an aqueous suspension of GO. Ascorbic acid (0.15 g) was added slowly to the GO suspension and stirred for 8 hours at 50°C. The product (rGO) was collected by centrifugation and washed several times with ethanol and dried at 80°C in a vacuum oven for 5 h.

For the synthesis of Fe_3O_4/rGO, a stable aqueous suspension of rGO was obtained after the ultrasonication of 0.025 g of rGO in 50 mL of distilled water for 1 h. This suspension was bubbled with nitrogen for 15 minutes and adjusted to pH 11-12 using NH_3. Then, $FeCl_2{\cdot}4H_2O$ (0.25 g) was added to the rGO suspension and stirred for 16 hours at ambient temperature. The final product (Fe_3O_4/rGO) was washed several times with ethanol and distilled water and dried at 80°C in a vacuum oven for 5 h.

2.4. Electrochemical Measurements. Prior to modification, the GCE was polished with 0.02 μm alumina powder to a mirror-like surface followed by sonication for about two minutes in double distilled water and dried at ambient temperature. Fe_3O_4/rGO or rGO material was first dispersed by means of ultrasonication in an analytical solvent (1.0 mg/mL) for 1 hour to get a suspension. Then, this suspension was mixed with the Nafion solution (1.25% in ethanol) in the ratio of 1 : 4 by volume. After that, 5 μL of the aliquot was cast onto the GCE. The solvent was evaporated using a dryer. After the modification, the electrode was washed with double distilled water and then left to dry in the air before the electrochemical studies were carried out. The modified electrodes were denoted as Fe_3O_4/rGO/Naf-GCE or rGO/Naf-GCE.

Cyclic voltammograms (henceforth CVs) were recorded from −0.50 V to +0.90 V (forward potential scan) and then from +0.90 mV to −0.5 V (reverse potential scan) at a scan rate of 0.10 V·s^{-1}. DP-ASV voltammograms were recorded from −0.5 V to +0.9 V at a scan rate of 0.02 V·s^{-1}. DP-ASV voltammograms of the blank solution (a solution of 0.1 M ABS pH 6 and double distilled water) were similarly recorded before each measurement. Panadol Extra (Sanofi-Synthelabo Company, Vietnam), Tiffy Dey (Thai Nakorn Patana Company Ltd., Vietnam), and pms-Mexcold (Imexpharm Corporation in technological cooperation with Pharmascience Inc., Canada) were employed in this study. The ten tablets of each analyzed pharmaceutical preparation were exactly weighed and finely ground in a mortar. An adequate amount of the powders was weighed and transferred to a 100-mL calibrated flask, which was completed to volume with the 0.1 M ABS buffer solution pH 6. The standard addition method was used for determining the pharmaceutical formulations.

3. Results and Discussion

3.1. Characterization of Materials. XRD measurements were used to study the phase of the obtained samples. Figure 1 shows the XRD patterns of GrO, rGO, and Fe_3O_4/rGO. The

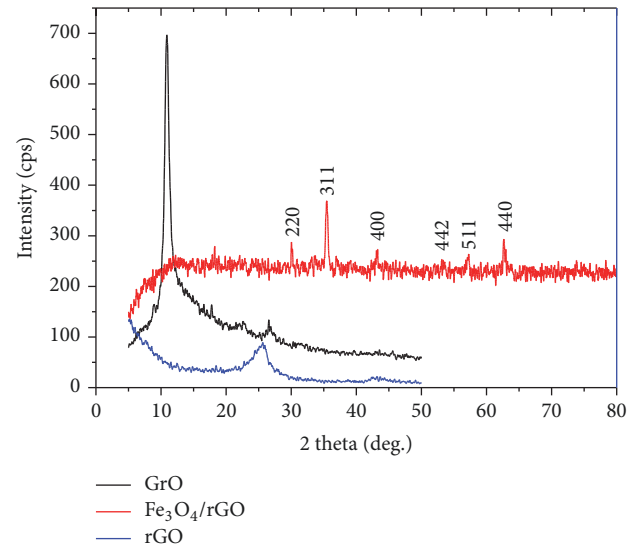

Figure 1: XRD patterns of GrO, rGO, and Fe_3O_4/rGO.

characteristic diffraction peak at the 2θ angle of around 11.3° of GrO was observed indicating that oxygen-containing functional groups on graphite sheets were formed, that is, the formation of GrO [34]. Two broad peaks at around 26° and 44° could be attributed to the initial graphite indicating that the oxidation of graphite was incomplete. In fact, a similar result is also obtained in reported papers [35, 36]. After reduced by ascorbic acid, the material does not show the peak at 11.3°, and the weak and broad reflection peak at 25.8° corresponds to the relative short-range order structures in disordered stacked rGO [37], which indicates the successful reduction of GrO. The diffractions at 2θ = 30.04°, 35.48°, 43.28°, 53.34°, and 62.68° for (220), (311), (400), (511), and (440) planes match Fe_3O_4 (JCPDS No. 19-0629) indicating that depositing magnetic iron oxide on rGO was successful.

In order to study the morphologies of rGO and Fe_3O_4/rGO, TEM images were recorded (Figure 2). The TEM images of rGO show a stacked and crumpled morphology due to the exfoliation and restacking process [37] (Figure 2(a)). It is difficult to obtain monodisperse Fe_3O_4 particles due to their inherent magnetism. However, the presence of rGO can prevent the aggregation of Fe_3O_4 nanoparticles. The highly dispersed Fe_3O_4 particles with small uniform single particles over the rGO sheet with an average particle size of 10–15 nm were observed (Figure 2(b)). The amount of iron analyzed by means of AAS was 36.5% compared to the theoretical amount of 57.5%. This may be due to the fact that iron has not been completely incorporated into rGO.

The existence of oxygen-containing functional groups was confirmed by FTIR (Figure 3). Upon the oxidation of graphite to GrO, the strong absorption band at 3414 cm^{-1} is attributed to ν_{OH}. The vibration bands located at 1724 cm^{-1} and 1616 cm^{-1} can be assigned to $\nu_{C=O}$ of carbonyl and $\nu_{C=C}$ of aromatic rings. The absorption bands at 1226 cm^{-1} and 1056 cm^{-1} belong to ν_{C-O} of epoxide and alkoxy, respectively [34, 38]. The vibrational band at 1400 cm^{-1} can be assigned to ν_{COO}. The presence of the oxidized groups (Figure 3(a))

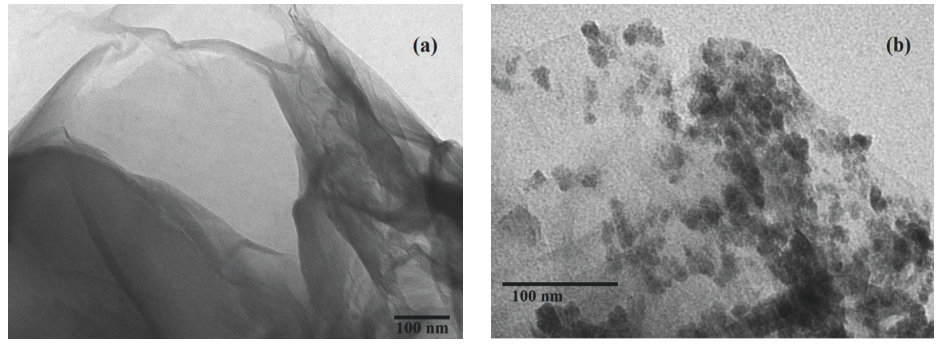

(a) (b)

Figure 2: TEM images of rGO (a) and Fe_3O_4/rGO (b).

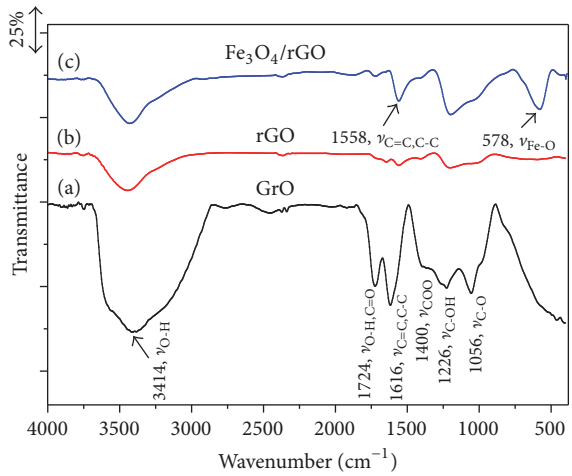

Figure 3: FTIR spectra of GrO, rGO, and Fe_3O_4/rGO.

indicates the successful oxidation of graphite to graphite oxide. In addition, the adsorption band of oxygen-containing functional groups was not observed (Figure 3(b)) indicating the reduction of GrO to form rGO. Furthermore, a new absorption band observed at 1558 cm^{-1} (Figure 3(c)) may belong to the skeletal vibration of graphene sheets [34]. The successful introduction of magnetic oxides onto rGO is confirmed by the sharp peak around 580 cm^{-1} assigned to Fe–O of Fe_3O_4 [39, 40].

The chemical state of the elements of Fe_3O_4/rGO is further confirmed by XPS. The XPS spectrum (Figure 4(a)) shows photoelectron lines implying the presence of three elements at a binding energy of 284, 530, and 720 eV corresponding to carbon (C_{1s}), oxygen (O_{1s}), and iron (Fe 2p), respectively. The high-resolution XPS for C_{1s} of rGO is shown in Figure 4(b). The deconvoluted C_{1s} spectrum implies that rGO consists of functional groups such as sp^3 (C–C, 282.2 eV), hydroxyl and epoxy (C=O, 284.2 eV), and carbonyl (C=O, 286.03 eV) [35]. The calculation of the atomic contributions shows the number of C–O and C=O groups on Fe_3O_4/rGO to be 43.8% and 16.0%, respectively, while maintaining the amount of C–C groups at 40.2%. The percentage of oxygen contained in the functional groups is rather high compared with that of other reports [41, 42], indicating that rGO was only partially reduced. Since XRD patterns of magnetite Fe_3O_4 and maghemite Fe_2O_3 are very similar [38], XPS Fe2p core level spectrum has been conducted to confirm magnetite (Figure 4(c)). A peak at 726.6 eV is attributed to 2p1/2 (Fe(III)) and the satellite peaks at 719.35 eV and 733.5 eV are characteristic for maghemite. The broad peaks of 2p3/2 Fe(II) at 713.1 eV and 2p1/2 Fe(III) at 724.75 eV are typical for magnetite [35]. Although nitrogen was bubbled during the synthesis process, a part of Fe(II) was oxidized by available oxidant agents (diluted oxygen, organic species in the oxidation form). Then, the mixture of Fe_3O_4 and Fe_2O_3 was obtained. The formation of Fe_3O_4/rGO and Fe_2O_3/rGO may be illustrated according to the following reactions:

$$\begin{aligned} &Fe^{2+} \xrightarrow{O_2,GO} Fe^{3+} \\ &2Fe^{3+} + Fe^{2+} + 8OH^- + rGO \\ &\qquad \xrightarrow{\text{Ambient temperature}} Fe_3O_4/rGO + 4H_2O \\ &2Fe^{3+} + 6OH^- + rGO \longrightarrow Fe_2O_3/rGO + 3H_2O \end{aligned} \tag{1}$$

The magnetic properties of Fe_3O_4/rGO were determined using VSM measurements at ambient temperature (Figure 5). The magnetization hysteresis loop has an S-like shape, and the saturation magnetization is 34 emu·g^{-1}. This value is lower than that of the pure nanomagnetic Fe_3O_4 [43] but compatible with that of Fe_3O_4/rGO reported in [38, 44, 45]. This low saturation magnetization of Fe_3O_4/rGO may be due to the relatively lower density of magnetic components in the Fe_3O_4/rGO nanocomposites. The magnetic coercivity was nearly zero indicating that there is no remaining magnetization upon the removal of the external magnetic field. Therefore, the superparamagnetic behavior of nanocomposite Fe_3O_4/rGO was confirmed.

The porous properties of GrO, rGO, and Fe_3O_4/rGO were investigated using the nitrogen adsorption-desorption isotherms (Figure 6). The isotherm curves belong to typical type IV according to IUPAC classification. The presence of the hysteresis loop at a high relative pressure region indicates the mesopore which was attributed to the void

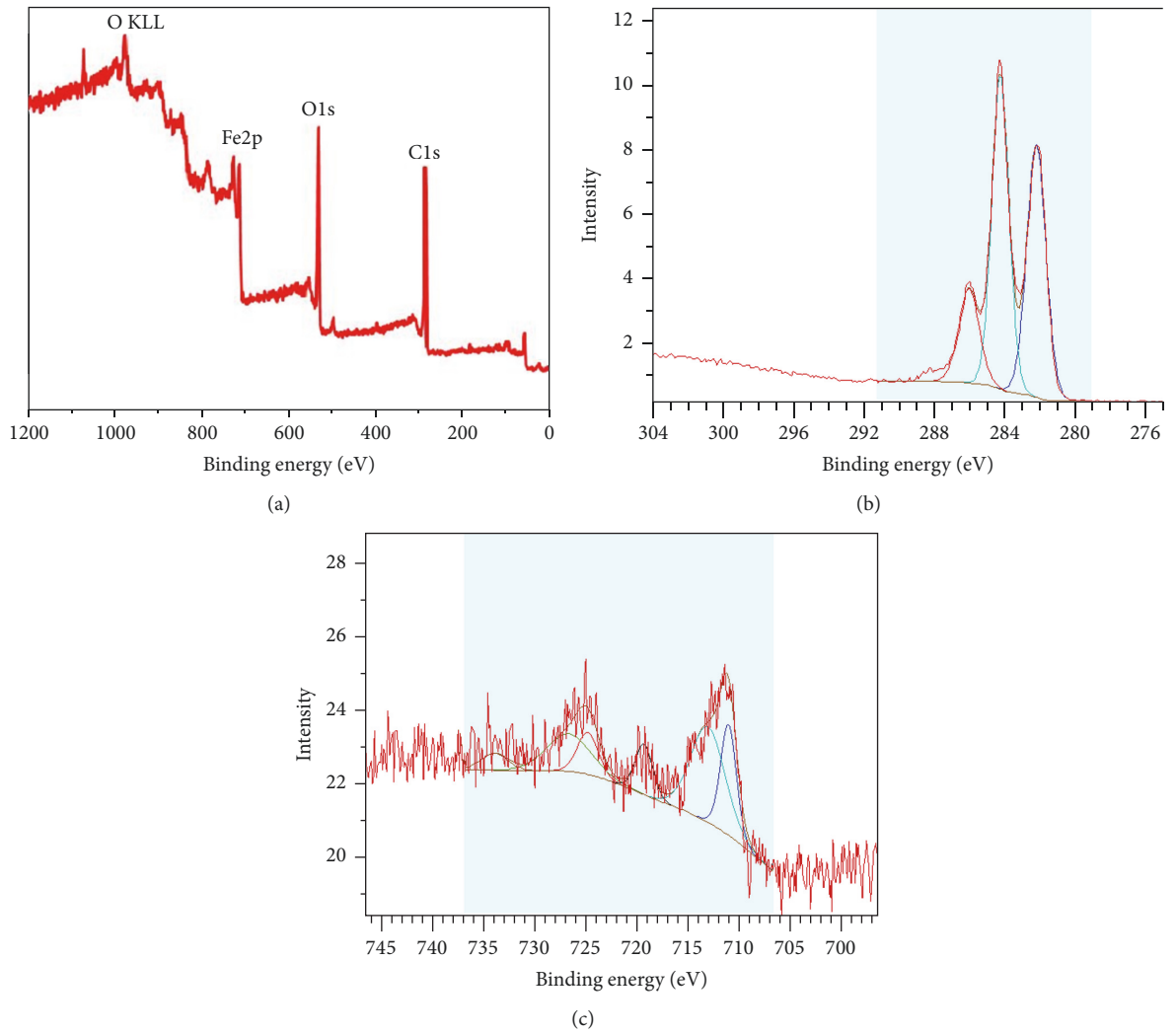

Figure 4: XPS spectra of (a) Fe_3O_4/rGO, (b) XPS core level spectrum of C_{1s}, (c) XPS core level spectrum of Fe_{2p}.

between the primary particles [46]. The specific surface areas calculated from the BET model of GrO, rGO, and Fe_3O_4/rGO are 81 m^2/g, 205.19 m^2/g, and 189.96 m^2/g, respectively. The reduction of the surface area of Fe_3O_4/rGO may be due to the aggregation of Fe_3O_4/rGO and the occupation of micropore by Fe_3O_4 introduced. The surface area of obtained Fe_3O_4/rGO is compatible with that of some reports [38, 44] but higher than that of other reports [47, 48].

The hydrophobic polyaromatic sheets of unoxidized benzene rings of rGO exhibit hydrophobic interaction and π–π stacks towards the organic molecules [49], while binding properties of iron oxides provide high reactivity. The Fe_3O_4/rGO composite with the combination of these properties is expected to be a potential electrode modifier for the determination of the organic compounds.

3.2. Electrochemical Performance of Fe_3O_4/rGO-Based Modified Electrodes

3.2.1. Preparation of Modified Electrode. The solvents used for dispersing the Fe_3O_4/rGO material significantly affect the peak current. Three solvents, namely, dimethylformamide (DMF), water, and ethanol, were selected to disperse Fe_3O_4/rGO. The CV curves of PRC are presented in Figure 7(a). As ethanol was used to disperse Fe_3O_4/rGO, the intensity of I_{ap} (anodic peak current) is 2.2 and 1.2 times higher than those in water and DMF, respectively. This indicates that ethanol is favorable for dispersing Fe_3O_4/rGO because it provides the highest I_{ap} with the lowest RSD_{ip} (relative standard deviation) equal to 0.9. Therefore, ethanol was selected as a dispersion solvent for further experiments.

The effect of pH on the voltammetric response of PRC was studied using CVs in the range of pH 4.8 to 9.8. The purpose of this study is to evaluate the ratio of electrons and protons participating in the voltammetric oxidation of PRC and also the optimum pH. The B-RBS buffer was used to adjust pH. Figure 7(b) shows the CVs recorded at different pH for the 2.10^{-4} M PRC solution. The anodic peak current increases with increasing pH from 4.8 to 6. A further increase in the pH leads to a decline of the current (inset of Figure 7(b)). Since pK_a of PRC in solution is 9.5 [18, 50], the form of PRC exists as negative species in the solution above 9.5 and positive

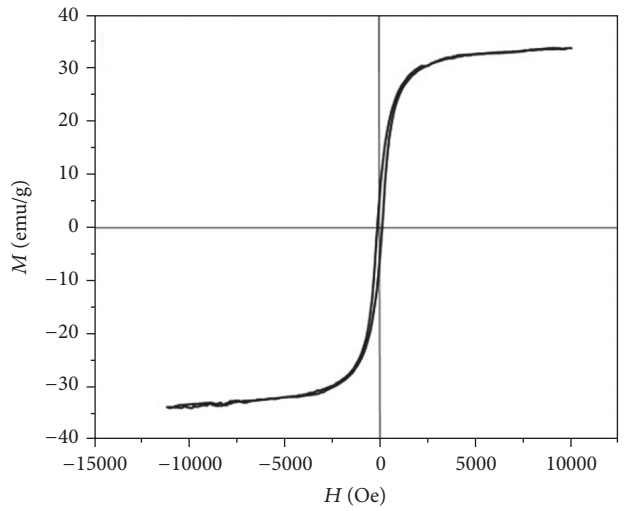

Figure 5: Magnetization curve of Fe_3O_4/rGO.

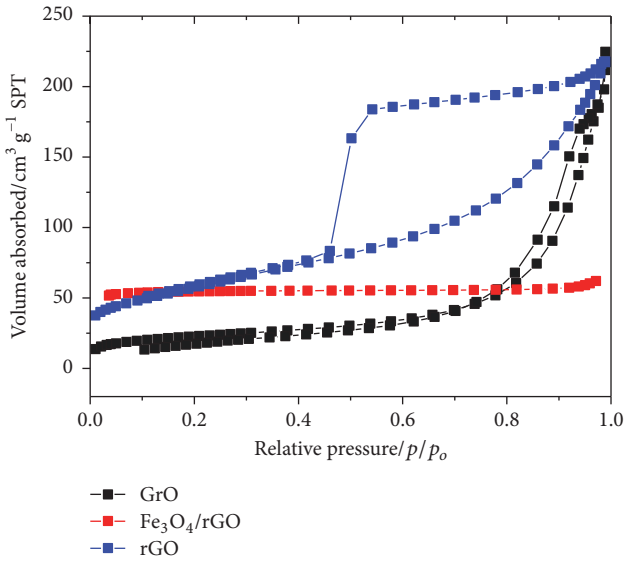

Figure 6: Nitrogen adsorption/desorption isotherms of GrO, rGO, and Fe_3O_4/rGO.

species below this pH. On the other hand, pH_{pzc} (point of zero charges) of Fe_3O_4/rGO is approximately 6.3 [33]. Therefore, the Fe_3O_4/rGO surface will be charged positively in the solution below pH_{pzc} and negatively above pH_{pzc}. The dependence of I_{ap} on pH can be explained as follows: at pH lower than pH_{pzc}, the peak current signal is low due to the positively charged surface repulsing the positive species of PRC. With the increase of pH, the positive charge of the surface decreases, and the electrostatic attraction results in a higher PRC stripping current. At pH higher than pH_{pzc}, the peak current signal is also low due to the negatively charged surface repulsing the negative species of PRC. The signal intensity is maximal at pH 6. Therefore, pH 6 was selected as the optimal pH.

The relationship between pH and the anodic peak potential, E_{ap}, is shown in the inset of Figure 7(b). As can be seen, the anodic peak shifts to more negative potentials with increasing pH from 4.8 to 9.8 indicating that protons associate directly with PRC oxidation. The linear regression equation can be expressed as

$$E_{ap} = 0.659 - 0.053 \cdot \text{pH}; \quad r = -0.997; \quad p < 0.001, \qquad (2)$$

where E_{ap} is the anodic peak potential, r is the correlation coefficient, and p is the significant value.

The linear relation between E_{ap} and pH was significant ($r = -0.997$, $p \leq 0.001$).

The slope of regression is (−0.053 V/pH) in excellent agreement with the potential shift predicted by the Nernst equation of −0.059 V/pH at 298 K. This indicates that the number of electrons and protons transferred in the redox reaction of PRC are equal.

Several buffers of pH 6 including ABS, CBS, PBS, UBS, and B-RBS were studied in order to evaluate the relevant buffer for the voltammetric response of PRC. Figure 7(c) shows the cyclic voltammograms recorded with different buffers. As can be seen from the figure, the ABS buffer with the lowest RSD (0.1%) provides the highest peak of the current signal. Then, ABS was selected as the buffer for further experiments.

Introducing Fe_3O_4/rGO on the surface of GCE considerably improved the electrochemical behaviors of PRC indicating that Fe_3O_4/rGO could play a critical role in the voltammetric response of PRC. Different amounts of Fe_3O_4/rGO suspension were investigated. The results showed that the peak current of PRC increased with increasing the volume of Fe_3O_4/rGO suspension introduced on the surface of GCE up to 5 μL (1 μg·mL^{-1}) (Figure 7(d)). It can be explained that as the Fe_3O_4/rGO amount increased, the accumulation efficiency of PRC on the modified GCE also increased, resulting in the peak current enhancement. However, a further increase of the Fe_3O_4/rGO amount caused a decrease of the anodic peak current of PRC. This can arise from the larger film thickness causing the increase of resistance of the modifier film against the electron transfer for PRC. As a result, $V = 5$ μL of Fe_3O_4/rGO suspension was chosen as an optimal amount.

3.2.2. Electrochemical Behavior of PRC on Modified Electrodes. The electrochemical experiments on the GCE modified with and without rGO or Fe_3O_4/rGO were conducted by CVs in order to confirm its electrochemical behavior of the modified GCE for the detection of PRC (Figure 8). The Nafion was introduced to improve the adhesion of Fe_3O_4/rGO and conductivity of the modified electrode. As can be seen from Figure 8, the current response on the bare GCE exhibited the broad peaks. After modifying the GCE by Nafion, rGO, or Fe_3O_4/rGO, the current responses on the modified electrodes provided the defined peaks, but that on the Fe_3O_4/rGO/Naf-GCE exhibited the well-defined stripping signal with the highest intensity.

The intensities of I_{ap} (anodic peak current) and I_{cp} (cathodic peak current) on Fe_3O_4/rGO/Naf-GCE are 1.7- and 1-fold, respectively, compared with that on the rGO/Naf-GCE. PRC exhibits a pair of well-defined redox waves on

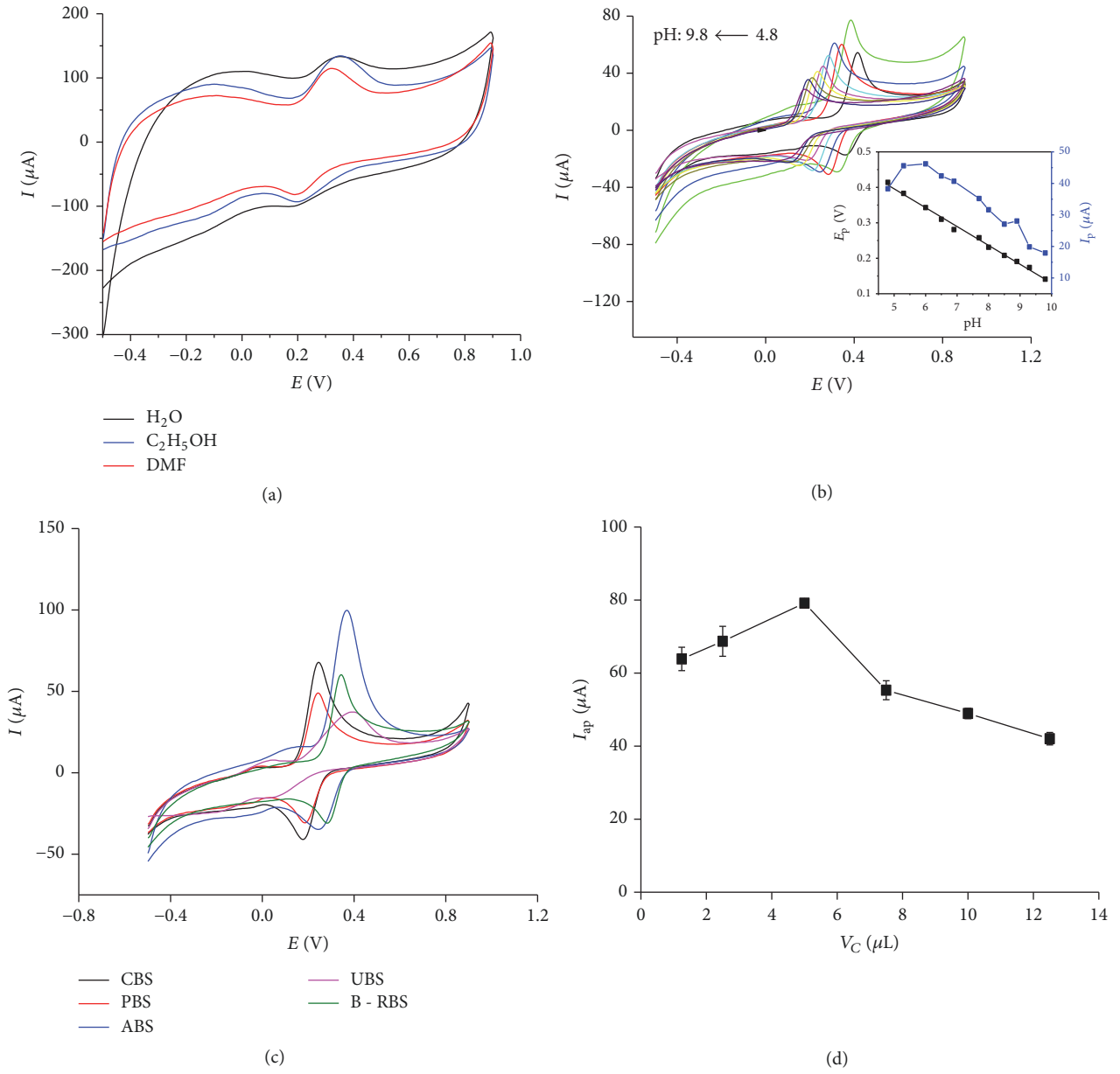

FIGURE 7: (a) CV curves of PRC with different solvents ($C_{PRC} = 3 \cdot 10^{-4}$ M, 0.1 M PBS pH 7, t_{acc} (accumulation time) = 60 s, scan rate = 0.1 V·s^{-1}, E_{acc} (accumulation potential) = 0.2 V); (b) CVs for PRC at Fe_3O_4/rGO/Naf-GCE in 0.05 M B-RBS with pH in the range from 4.8 to 9.8. Inset presents the plots of potential and current of PRC peaks versus pH values; (c) CVs for PRC in different buffer solutions pH 6 ($C_{PRC} = 3 \cdot 10^{-4}$ M, t_{acc} = 60 s, scan rate = 0.1 mV·s^{-1}, E_{acc} = 0.2 V); (d) I_{ap} of PRC using different amounts of Fe_3O_4/rGO for modified electrode ($C_{PRC} = 3 \cdot 10^{-4}$ M, 0.1 M ABS pH 6, t_{acc} = 60 s, scan rate = 0.1 V·s^{-1}, E_{acc} = 0.2 V).

the Fe_3O_4/rGO modified GCE with E_{ap} = 0.37 V and E_{cp} = 0.25 V. The favorable signal-promoting effect of Fe_3O_4/rGO indicated that it could enhance the electron transfer rate of PRC and had a good electrocatalytic activity for the *redox* reaction of PRC. The favorable formed π–π interaction between the PRC molecules and the rGO sheets of sp^2-bonded carbon atoms with strengthening adsorption [51] were possibly responsible for the accumulation of PRC. In addition, the coordination of the nitrogen atoms in PRC with the Fe(II) and Fe(III) ions in Fe_3O_4/rGO also contributed to the attracting of the analytes to the electrode surface. The combinations of these effects led to a greater amount of PRC accumulation on the surface of Fe_3O_4/rGO/Naf-GCE, greatly improving the PRC voltammetric signal.

3.2.3. Factors Affecting the Stripping Voltammetric Signals

(1) Effect of Scan Rate. Important information about electrochemical mechanism can usually be obtained from the relationship between the voltammetric responses and the scan rate. Therefore, the effects of scan rate on the peak potential (anodic peak potential (E_{ap}), cathodic peak potential (E_{cp}))

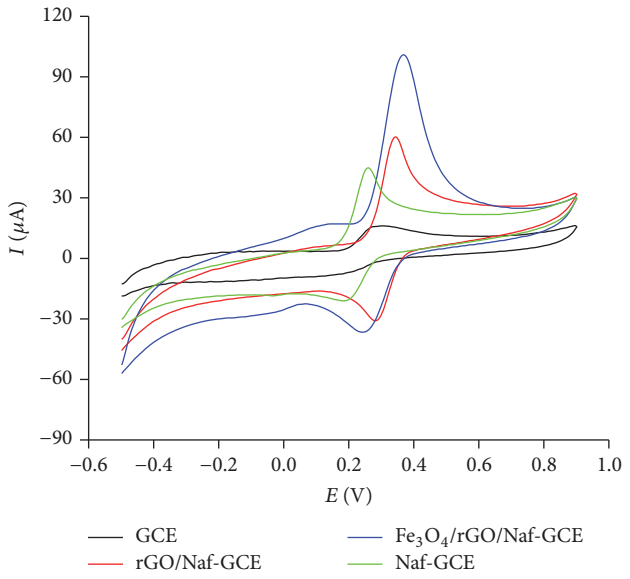

Figure 8: CV curves for PRC at the bare GCE, Naf-GCE, rGO/Naf-GCE, and Fe_3O_4/rGO/Naf-GCE ($C_{PRC} = 3 \times 10^{-4}$ M, 0.1 M ABS pH 6, $t_{acc} = 60$ s, scan rate = 0.1 V·s^{-1}, $E_{acc} = 0.2$ V).

and peak current (I_{ap} and I_{cp}) were investigated using the CV method (Figure 9(a)). As seen in Figure 9(a), E_p increased with an increase in the scan rate. Such dependence of E_p on the scan rate indicated that the homogeneous electron transfer in PRC oxidation is irreversible [52]. Peak current (I_{ap} and I_{cp}) in Figure 9(b) increased with an increase in the scan rate within 0.2–0.5 V·s^{-1} suggesting that the electron transfer reaction is involved with a surface-confined process [53].

In order to determine if the electrooxidation reaction is adsorption or diffusion controlled, the plots of peak current (I_p) against the square root of the scan rate ($v^{1/2}$) and $\ln I_p$ against $\ln v$ were drawn (Figures 9(b) and 9(c)). If the plot of I_p versus $v^{1/2}$ is linear and intercepting the origin, this process is controlled by diffusion [52]. In the range from 0.2 V·s^{-1} to 0.5 V·s^{-1}, I_p of PRC electrooxidation and electroreduction varied linearly according to $v^{1/2}$ and was expressed by the following equations:

$$\begin{aligned} I_{ap} &= (-6.82 \pm 11.87) + (8.11 \pm 0.86) \cdot v^{1/2}; \\ &\qquad r = 0.997, \ p < 0.001, \\ I_{cp} &= (-3.90 \pm 5.17) + (2.74 \pm 0.37) \cdot v^{1/2}; \\ &\qquad r = 0.995, \ p < 0.001. \end{aligned} \tag{3}$$

The plots of I_p with $v^{1/2}$ (Figure 9(b)) are highly linear ($p \le 0.001$). With significant level, $\alpha = 0.05$, the intercepts of I_{ap} and I_{cp} cross the origin because 95% confident intervals (-6.82 ± 11.87) for I_{ap} and (-3.90 ± 5.17) for I_{cp} contain zero. It means that the electrode process of PRC electrooxidation and electroreduction is controlled by diffusion.

On the other hand, the plot of the linear regression line for $\ln I_p$ and $\ln v$ can provide the information about diffusion- or adsorption-controlled process. The slope near 1 is attributed to the adsorption-controlled electrode process and that near 0.5 is said to be a diffusion-controlled process [14]. Both linear relationships with high relative coefficients ($p \le 0.001$) were obtained (Figure 9(c)) and expressed by the following equations:

$$\begin{aligned} \ln I_{ap} &= 1.70 + 0.56 \cdot \ln(v); \quad r = 0.995, \ p < 0.001, \\ \ln I_{cp} &= 0.36 + 0.60 \cdot \ln(v); \quad r = 0.987, \ p < 0.001. \end{aligned} \tag{4}$$

Its slopes of 0.56 and 0.60 are close to 0.5, again asserting that the redox process of PRC on the modified electrode was controlled by the diffusion.

The electron transfer coefficient (α) and the electron transfer rate constant (k_s) were calculated based on the Laviron equation [54].

For the anodic process

$$\begin{aligned} E_{ap} = E^0 &+ \frac{R \cdot T}{n \cdot F \cdot (1-\alpha)} \cdot \ln \frac{n \cdot F \cdot (1-\alpha)}{R \cdot T \cdot k_s} \\ &+ \frac{R \cdot T}{n \cdot F \cdot (1-\alpha)} \cdot \ln v, \end{aligned} \tag{5}$$

where n is the number of transfer electrons, E^0 is the formal redox potential, $R = 8.314$ J·mol^{-1}·K^{-1}, $T = 298$ K, and $F = 96500$ C·mol^{-1} at 298 K

For the cathodic process

$$E_{cp} = E^0 - \frac{R \cdot T}{n \cdot F \cdot \alpha} \cdot \ln \frac{n \cdot F \cdot \alpha}{R \cdot T \cdot k_s} - \frac{R \cdot T}{n \cdot F \cdot \alpha} \cdot \ln v. \tag{6}$$

The plots of peak potentials (E_{ap} and E_{cp}) against $\ln v$ are shown in Figure 9(d). The linear regression equations are expressed as follows:

$$E_{ap} = 0.430 + 0.027 \cdot \ln v; \quad r = 0.991; \ p < 0.001, \tag{7}$$

$$E_{cp} = 0.208 - 0.018 \cdot \ln v; \quad r = 0.991; \ p < 0.001. \tag{8}$$

From (5), (6), (7), and (8), the electron transfer coefficient and electron transfer rate constant can be calculated as 0.595 and 0.315 s^{-1}, respectively. On the other hand, combining (5) and (7), the value of $(1-\alpha) \cdot n$ can be calculated as 0.93. Therefore, the average value of the number of electron transferred (n) was 2.3. Consequently, assuming $n = 2$ for PRC, the oxidation mechanisms for PRC involve two electrons and two protons and are likely to be in agreement with those reported in other papers [55, 56]. The oxidation of PRC leads to a quinine type moiety as proposed earlier [57] (Scheme 1).

An approximate evaluation of the amount of adsorbed PRC on modified GCE (surface coverage of the electrode) can be obtained by using the method proposed by Sharp et al. [58]. The I_{ap} is a function of the surface concentration of electroactive species and calculated according to the following equation:

$$I_{ap} = \frac{n^2 \cdot F^2 \cdot A \cdot \Gamma \cdot \nu}{4 \cdot R \cdot T}, \tag{9}$$

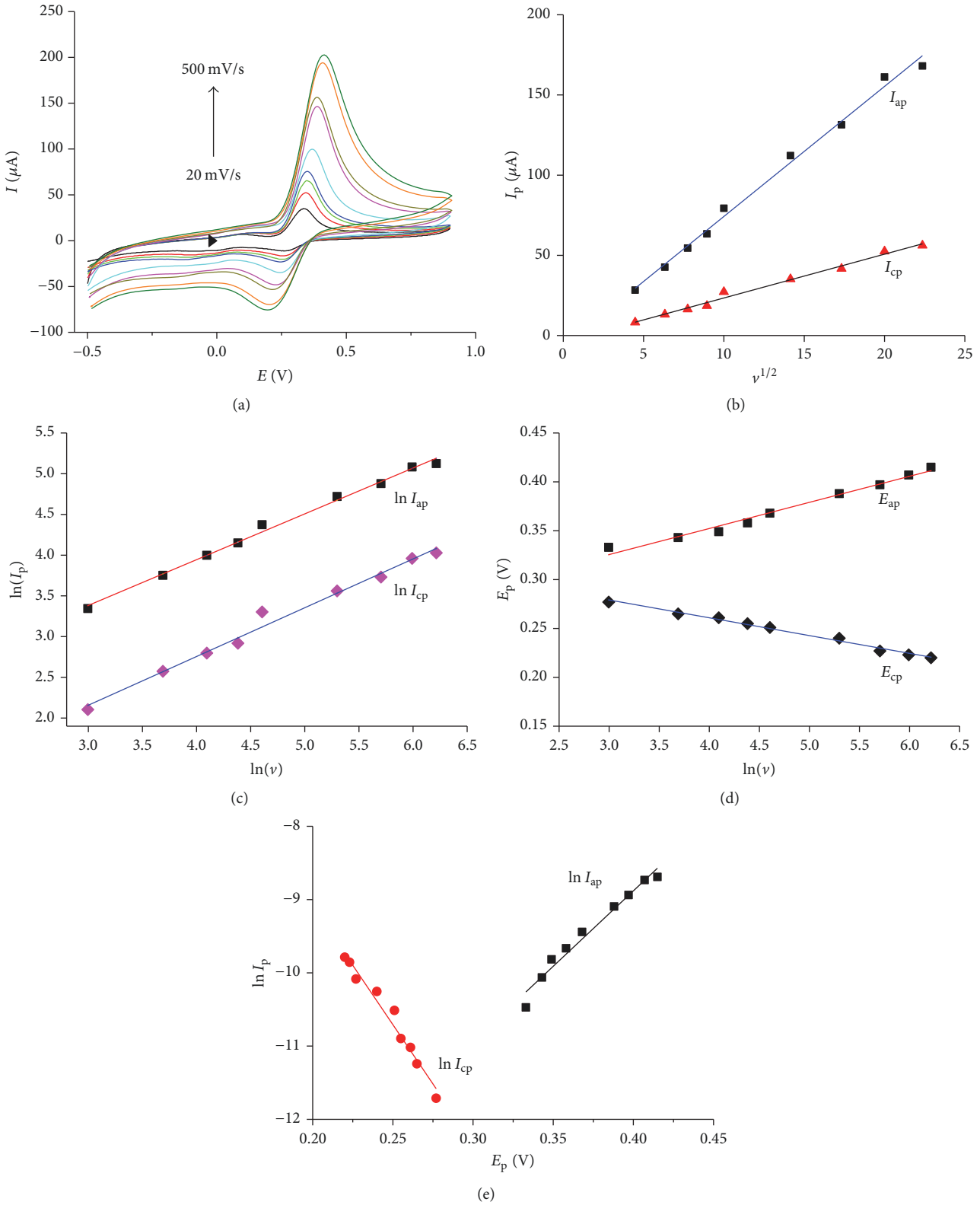

FIGURE 9: (a) CVs for $3 \cdot 10^{-4}$ M PRC on Fe_3O_4/rGO/Naf-GCE in 0.1 M ABS pH 6 in scan rates (v) from 0.02 V·s^{-1} to 0.5 V·s^{-1}; (b) dependence of anodic peak current (I_{ap}) and cathodic peak current (I_{cp}) on $v^{1/2}$; (c) plot of ln I_{ap} and ln I_{cp} against ln v; (d) linear regression between anodic peak potential (E_{ap}) and cathode peak potential (E_{cp}) versus ln v; (e) plot of ln I_p versus of E_p.

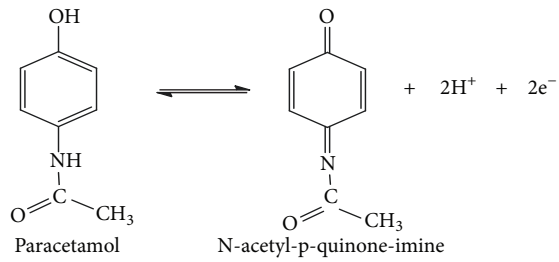

Scheme 1: The oxidation reaction for PRC.

where n is the number of electrons involved in the reaction, A is the surface geometrical area (0.062 cm^2), and Γ ($mol{\cdot}cm^{-2}$) is the surface coverage. From the slope of the anodic peak currents (I_{ap}) versus the scan rate, the surface coverage was calculated as 4.1×10^{-6} $mol{\cdot}cm^{-2}$ for PRC on the surface of Fe_3O_4/rGO/Naf-GCE.

The effective surface area of the modified electrode could be obtained based on the current-potential characteristics. According to Bard and Faulkner's equation [52, 59], the relation between current and potential of the oxidation irreversible process is described by the following equation:

$$I_{ap} = 0.227 \cdot F \cdot A \cdot C \cdot \exp\left(\frac{\alpha F}{RT} \cdot E_p\right), \quad (10)$$

where I_{ap} is peak current (A), E_p is the peak potential (V); A is an active surface area (cm^2); C is the bulk concentration of PRC (3×10^{-7} $mol^{-1}{\cdot}cm^3$); and other parameters were defined above.

Taking natural logarithm of (10), one obtained the dependence below:

$$\ln I_p = \ln (0.227 \cdot F \cdot A \cdot C) + \frac{\alpha \cdot F}{R \cdot T} \cdot E_p. \quad (11)$$

The plot of linear regression between $\ln I_p$ and E_p was established (Figure 9(e)). The active surface area of the modified electrode obtained from the intercept of the linear regression line was 5.6 cm^2. The geometry surface area of electrode is 0.065 cm^2 (diameter of electrode = 2.8 mm). The effective surface area was 86 times larger compared with the geometry surface area of the electrode. The increase of surface of the modified electrode is due to the presence of Fe_3O_4/rGO. The larger effective surface area results in more active sites and leads to a higher signal to noise ratio.

(2) Effect of Pulse Amplitude (ΔE), Accumulation Potential, and Time. Pulse amplitudes significantly affect the voltammetric stripping signal of the analytes. The pulse amplitude in the range of 0.04 V to 0.20 V was studied using the DP-ASV method. The results showed that I_p increased linearly and E_p shifted negatively as pulse amplitudes increased (Figure 10(a)). As ΔE was larger than 0.1 V, the peak width of the current peak tends to be wide, reducing the peak resolution and hence the selectivity. The pulse amplitude of 0.10 V that provided a symmetric peak with low RSD (1.8%) was selected for the next experiments (inset of Figure 10(a)).

The influence of accumulation potential and time on the I_p of PRC at Fe_3O_4/rGO was also investigated using the DP-ASV method in the range of −0.1 V to 0.5 V (Figures 10(b) and 10(c)). The I_{ap} increased as the potential shifted positively from −0.1 V to 0 mV and reached a maximum at 0 V; then it decreased as the potentials shifted positively from 0 V to 0.5 V. A potential of 0.0 V was selected as the optimal accumulation potential. The accumulation time also had an effect on the peak current. The I_p increased slightly with time, peaked at 75 s, and then decreased afterwards. Therefore, 75 s was used as the accumulation time (Figure 10(c)).

(3) Effect of Interferents. The effect of possible interferents was investigated by adding some compounds to a solution containing 1×10^{-4} $mol{\cdot}L^{-1}$ PRC in the 0.1 M ABS (pH = 6). Ascorbic acid (AA), uric acid (UA), and caffeine (CF) are commonly present in pharmaceutical samples, and they were tested as interferents at different molar ratios of the referent to PRC (0.5/1; 1/1 and 2/1 for AA and UA, and 5/1; 10/1 and 20/1 for CF). I_p in the presence of the interferents was recorded and compared with I_p without interferent. The relative error (Re) did not exceed 5%, indicating that the Fe_3O_4/rGO/Naf-GCE can be employed for the determination of PRC in the presence of AA, UA, and CF (Table 1).

3.2.4. Repeatability, Reproducibility, and Limit of Detection (LOD). The repeatability of Fe_3O_4/rGO/Naf-GCE for DP-ASV was checked with different PRC concentrations (6×10^{-6} M, 10×10^{-6} M and 40×10^{-6} M). Each signal was measured nine times successively. The obtained RSDs for the 6×10^{-6} M, 10×10^{-6} M, and 40×10^{-6} M solutions were 0.12, 0.12, and 0.34%, respectively, lower than $(1/2) \cdot \mathrm{RSD}_{\text{Horwitz predicted}}$ [60]. Such reasonable RSDs of successive measurements indicated that Fe_3O_4/rGO/Naf-GCE could be repeatedly used for the detection of PRC in either low concentration range or high concentration range.

The dependence of the anodic stripping current (I_{ap}) for PRC on its concentration was conducted using DP-ASV (Figure 11(a)). The (I_{ap}) of PRC versus its concentrations exhibited a nonlinear response in the concentration range of 2–150 μM (the insert of Figure 11(a)). From the plot of I_p versus added concentrations of PRC, two ranges were obtained (Figure 11(b)). The first linear range between 2 μM and 10 μM and the second range between 10 μM and 150 μM were described in the following equations:

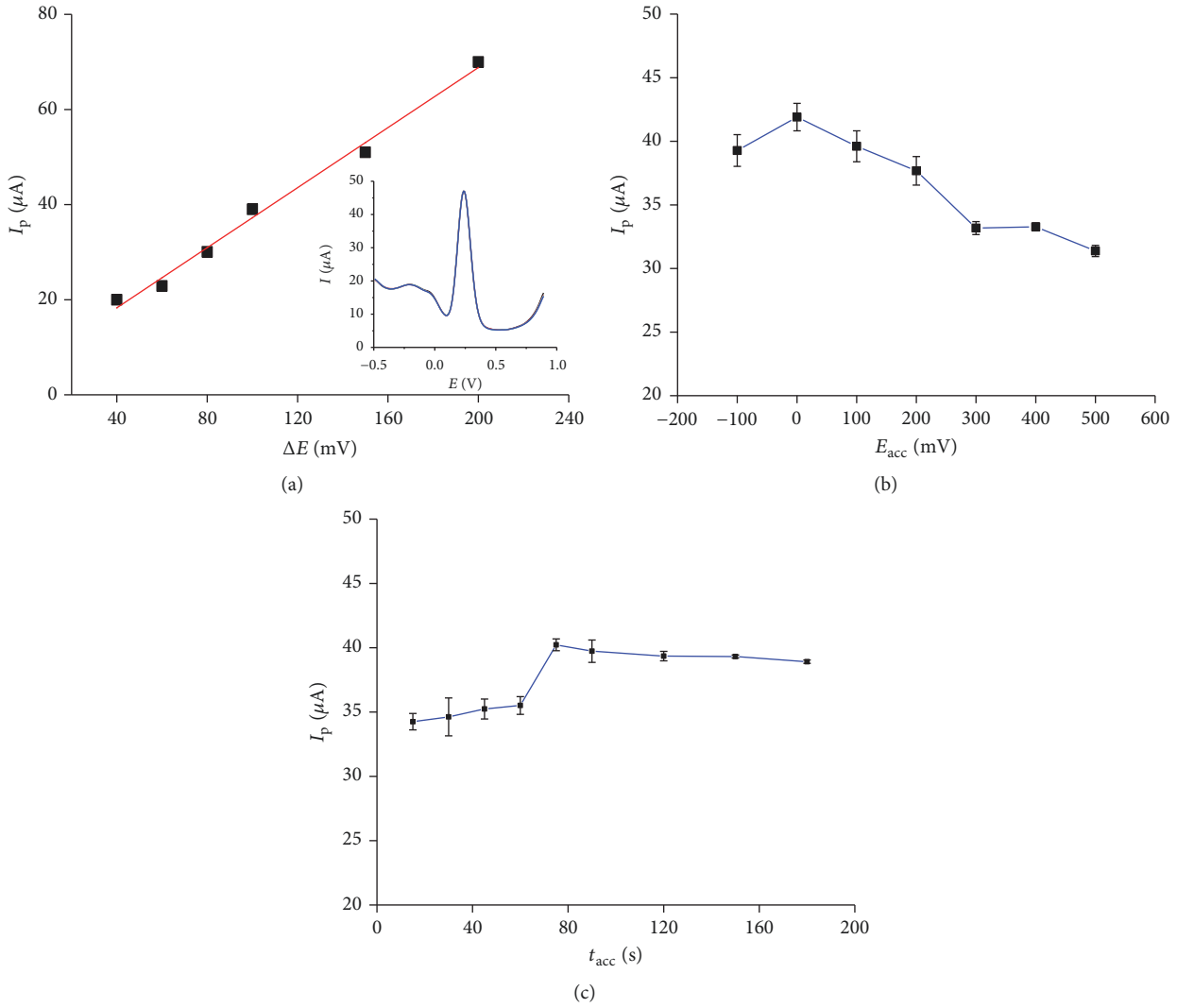

FIGURE 10: (a) The dependence of I_{ap} for PRC ($C_{PAR} = 10^{-4}$ M) in 0.1 ABS buffer pH 6 on pulse amplitude (ΔE); inset shows DP-ASV curves of PRC at $\Delta E = 0.1$ V; (b) on the accumulation potential (E_{acc}); (c) on accumulation time (t_{acc}).

TABLE 1: Effect of interferents on peak current of PRC at Fe_3O_4/rGO/Naf-GCE.

Ascorbic acid			Uric acid			Caffeine		
[AA]/[PRC]	$I_{p,PAR}$ (μA)	Re* (%)	[UA]/[PRC]	$I_{p,PAR}$ (μA)	Re* (%)	[CF]/[PRC]	$I_{p,PAR}$ (μA)	Re* (%)
0	36.27	0	0	34.12	0	0	39.93	0
0.5	36.18	0.25	0.5	34.00	0.34	5	39.51	1.06
1.0	35.95	0.89	1.0	33.70	1.22	10	*38.91*	*2.56*
2.0	35.46	2.23	2.0	*32.52*	*4.67*	20	*38.31*	*4.06*

Re = 100 × (I_p without interferent − I_p in presence of interferent)/I_p without interferent. *Average of 3 measurements.

$$I_{p,1} = -0.4114 + 0.5128 \cdot C_{PRC}; \quad r = 0.999; \ p < 0.001, \quad (12)$$

$$I_{p,2} = 4.383 + 0.261 \cdot C_{PRC}; \quad r = 0.994; \ p < 0.001.$$

The break in the calibration curve of PRC probably reflects the formation of a submonolayer in the first range of calibration and the formation of a monolayer in the second range as proposed by Kachoosangi et al. [18]. The limit of detection (LOD) calculated in the first range of the PRC concentrations (2–10 μM) was 0.72×10^{-6} M. The obtained LOD in this work was comparable with that in other references, in which the electrode was modified with dipyrromethene–Cu(II) monolayers, PAY/nano-TiO_2,

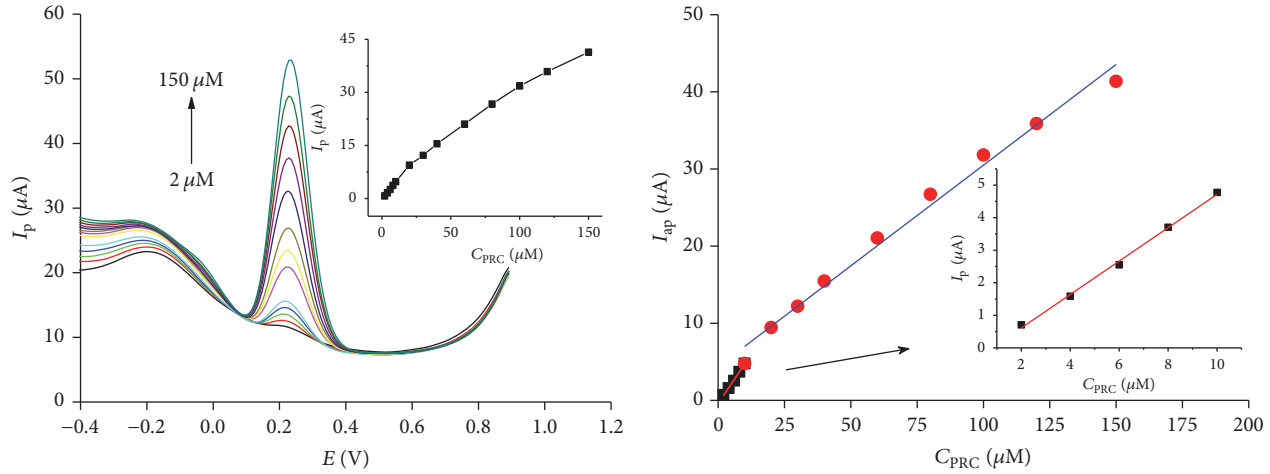

Figure 11: (a) DP-ASV curves of PRC on its concentration in the range of 2 μM to 150 μM in 0.1 M ABS buffer pH 6; the inset presents the plot of I_{ap} versus C_{PRC}; (b) double-linear regression of I_{ap} versus concentrations; the inset shows the linear regression line of the first segment (t_{acc} = 75 s, scan rate = 0.01 V·s^{-1}, E_{acc} = 0 V, ΔE = 0.1 V).

Table 2: Comparison of the Fe_3O_4/rGO modified GCE with the reported methods for the determination of paracetamol.

Electrode modifiers	Method	pH used	LOD (M)	References
Fe_3O_4/rGO	DP-ASV	6.0	7.2×10^{-7}	Proposed method
Dipyrromethene–Cu(II) monolayers	OSWV	7.0	1.3×10^{-4}	53
PAY/nano-TiO_2/GC electrode	DPV	7.0	2×10^{-6}	54
Cu(II)-conducting polymer complex	CV	7.0	5×10^{-6}	55
MWCNTs	DPV/CV	7.0	7.1×10^{-6}	56
AuNP-PGA/SWCNT	CV	7.2	1.18×10^{-6}	57
Carbon-coated nickel magnetic nanoparticles	DPV	3.0	6×10^{-7}	58
Graphene	SWV	7.5	3.2×10^{-8}	17
SWCNTs	OSWV	7.2	2.9×10^{-9}	59
MWCNTs	CV	7.5	1×10^{-9}	18

PAY: poly(acid yellow 9), SWV: square wave voltammetry; OSWV: Osteryoung square wave voltammetry, MWCNT: multiwalled carbon nanotube; SWCNT: single-walled carbon nanotubes.

Cu(II)-conducting polymer complex, single-walled carbon nanotubes, and multiwalled carbon nanotube [17, 18, 61] (Table 2). It could be noticed that LOD of PRC from the proposed method was lower than or comparable with those results based on modified electrodes in previous papers. The Fe_3O_4/rGO modified electrode performed better than some of the electrodes based on PAY/nano-TiO_2, Cu(II)-conducting polymer complex, and so on but failed to some others. Overall, the Fe_3O_4/rGO was proved to be an effective electrode modifier for the detection of PRC.

3.2.5. Determination of PRC in Real Samples. The proposed method was used to determine three kinds of PRC commercial tablets, namely, Panadol Extra (Sanofi-Synthelabo Company, Vietnam), Tiffy Dey (Thai Nakorn Patana Company Ltd, Vietnam), and pms-Mexcold (Imexpharm Corporation in technological cooperation with Pharmascience Inc., Canada). The tablets were ground to powder and dissolved in distilled water. The PRC concentration was analyzed using the DP-ASV method. The recoveries of the tests performed using DP-ASV were in the range from 95.5% to 107.0% for all the three samples. This result suggested that the determination of PRC applying the DP-ASV with Fe_3O_4/rGO/Naf-GCE possessed an acceptable error [62]. Table 3 also presents the values of the amounts of PRC determined using the HPLC method for the sake of comparison. The paired samples t-test was applied to estimate the data statistically. With the significant level of α = 0.05, the amounts of PRC analyzed with the proposed method are in good agreement with the content of PRC provided in the labels ($t_{(2)}$ = −1.066, p = 0.395 > 0.05). No significant differences were observed between the values determined with the proposed method and the HPLC method for the amount of PRC in the tablets ($t_{(2)}$ = −0.851, p = 0.851 > 0.05). These results indicate that the electrode developed in this work is relevant for detecting PRC in commercial tablets.

Table 3: Results obtained in the determination of paracetamol in pharmaceutical formulations using the DP-ASV and HPLC.

Sample	Tablet label value (mg)	HPLC value* (mg)	DP-ASV value* (mg)	Rev.	Re
Panadol Extra	500	502.75	496.86	95.2	1.2
Tiffy Dey	500	494.50	505.63	103.8	–2.3
pms-Mexcold	500	501.20	509.37	107.0	–1.6

* Average of 3 measurements. Re(%) = 100 × (DP-ASV value − HPLC value)/HPLC value.

4. Conclusions

Fe_3O_4/rGO was synthesized using a facile one-step process. The magnetic iron oxide with very fine spherical particles in nanoscales was highly dispersed on the rGO sheets. Fe_3O_4/rGO possessed superparamagnetic properties at room temperature and the saturation magnetization approaches 34 emu·g^{-1}. The Fe_3O_4/rGO-based electrode has been developed, and it exhibits an excellent electrocatalytic activity towards the reduction and oxidation of PRC. Fe_3O_4/rGO-based GCE promotes the sensitivity of the determination of PRC with a low detection limit (0.72×10^{-6} M). The analytical response was unaffected by the presence of caffeine, ascorbic acid, and uric acid commonly found in commercially available pharmaceutical tables. We also demonstrated the application of Fe_3O_4/rGO for the determination of PRC in pharmaceutical preparations with satisfactory results.

Conflicts of Interest

The authors declare that they have no conflicts of interest.

References

[1] R. N. Goyal and S. P. Singh, "Voltammetric determination of paracetamol at C60-modified glassy carbon electrode," *Electrochimica Acta*, vol. 51, no. 15, pp. 3008–3012, 2006.

[2] M. Kartal, "LC method for the analysis of paracetamol, caffeine and codeine phosphate in pharmaceutical preparations," *Journal of Pharmaceutical and Biomedical Analysis*, vol. 26, no. 5-6, pp. 857–864, 2001.

[3] M. Li and L. Jing, "Electrochemical behavior of acetaminophen and its detection on the PANI-MWCNTs composite modified electrode," *Electrochimica Acta*, vol. 52, no. 9, pp. 3250–3257, 2007.

[4] J. T. Franeta, D. Agbaba, S. Eric, S. Pavkov, M. Aleksic, and S. Vladimirov, "HPLC assay of acetylsalicylic acid, paracetamol, caffeine and phenobarbital in tablets," *Farmaco*, vol. 57, no. 9, pp. 709–713, 2002.

[5] G. M. Hadad, S. Emara, and W. M. M. Mahmoud, "Development and validation of a stability-indicating RP-HPLC method for the determination of paracetamol with dantrolene or/and cetirizine and pseudoephedrine in two pharmaceutical dosage forms," *Talanta*, vol. 79, no. 5, pp. 1360–1367, 2009.

[6] N. Pejić, L. Kolar-Anić, S. Anić, and D. Stanisavljev, "Determination of paracetamol in pure and pharmaceutical dosage forms by pulse perturbation technique," *Journal of Pharmaceutical and Biomedical Analysis*, vol. 41, no. 2, pp. 610–615, 2006.

[7] M. J. Gómez, M. Petrović, A. R. Fernández-Alba, and D. Barceló, "Determination of pharmaceuticals of various therapeutic classes by solid-phase extraction and liquid chromatography-tandem mass spectrometry analysis in hospital effluent wastewaters," *Journal of Chromatography A*, vol. 1114, no. 2, pp. 224–233, 2006.

[8] T. Madrakian, A. Afkhami, and M. Mohammadnejad, "Second-order advantage applied to simultaneous spectrofluorimetric determination of paracetamol and mefenamic acid in urine samples," *Analytica Chimica Acta*, vol. 645, no. 1-2, pp. 25–29, 2009.

[9] L. Yu, H. Wu, B. Wu et al., "Magnetic Fe3O4-Reduced Graphene Oxide Nanocomposites-Based Electrochemical Biosensing," *Nano-Micro Letters*, vol. 6, no. 3, pp. 258–267, 2014.

[10] S. J. R. Prabakar and S. S. Narayanan, "Amperometric determination of paracetomol by a surface modified cobalt hexacyanoferrate graphite wax composite electrode," *Talanta*, vol. 72, no. 5, pp. 1818–1827, 2007.

[11] W. Ruengsitagoon, S. Liawruangrath, and A. Townshend, "Flow injection chemiluminescence determination of paracetamol," *Talanta*, vol. 69, no. 4, pp. 976–983, 2006.

[12] S. Zhao, W. Bai, H. Yuan, and D. Xiao, "Detection of paracetamol by capillary electrophoresis with chemiluminescence detection," *Analytica Chimica Acta*, vol. 559, no. 2, pp. 195–199, 2006.

[13] L. Xiao, H. Xu, S. Zhou et al., "Simultaneous detection of Cd(II) and Pb(II) by differential pulse anodic stripping voltammetry at a nitrogen-doped microporous carbon/Nafion/bismuth-film electrode," *Electrochimica Acta*, vol. 143, pp. 143–151, 2014.

[14] S. Chitravathi and N. Munichandraiah, "Voltammetric determination of paracetamol, tramadol and caffeine using poly(Nile blue) modified glassy carbon electrode," *Journal of Electroanalytical Chemistry*, vol. 764, pp. 93–103, 2016.

[15] D. Q. Khieu, B. H. D. Son, V. T. T. Chau, P. D. Du, N. H. Phong, and N. T. D. Chau, "3-Mercaptopropyltrimethoxysilane Modified Diatomite: Preparation and Application for Voltammetric Determination of Lead (II) and Cadmium (II)," *Journal of Chemistry*, vol. 2017, Article ID 9560293, 2017.

[16] Y. Wang, H. Ge, Y. Wu, G. Ye, H. Chen, and X. Hu, "Construction of an electrochemical sensor based on amino-functionalized metal-organic frameworks for differential pulse anodic stripping voltammetric determination of lead," *Talanta*, vol. 129, pp. 100–105, 2014.

[17] X. Kang, J. Wang, H. Wu, J. Liu, I. A. Aksay, and Y. Lin, "A graphene-based electrochemical sensor for sensitive detection of paracetamol," *Talanta*, vol. 81, no. 3, pp. 754–759, 2010.

[18] R. T. Kachoosangi, G. G. Wildgoose, and R. G. Compton, "Sensitive adsorptive stripping voltammetric determination of paracetamol at multiwalled carbon nanotube modified basal plane pyrolytic graphite electrode," *Analytica Chimica Acta*, vol. 618, no. 1, pp. 54–60, 2008.

[19] M. Zidan, T. W. Tee, A. H. Abdullah, Z. Zainal, and G. J. Kheng, "Electrochemical oxidation of paracetamol mediated by

nanoparticles bismuth oxide modified glassy carbon electrode," *International Journal of Electrochemical Science*, vol. 6, no. 2, pp. 279–288, 2011.

[20] E. R. Vago and E. J. Calvo, "Electroreduction of oxygen on Fe3O4 electrodes. Part 2. - Rotating ring-disc electrode studies and mechanism," *Journal of the Chemical Society, Faraday Transactions*, vol. 91, no. 15, pp. 2323–2329, 1995.

[21] S. Stankovich, R. D. Piner, X. Chen, N. Wu, S. T. Nguyen, and R. S. Ruoff, "Stable aqueous dispersions of graphitic nanoplatelets via the reduction of exfoliated graphite oxide in the presence of poly(sodium 4-styrenesulfonate)," *Journal of Materials Chemistry*, vol. 16, no. 2, pp. 155–158, 2006.

[22] R. Muszynski, B. Seger, and P. V. Kamat, "Decorating graphene sheets with gold nanoparticles," *The Journal of Physical Chemistry C*, vol. 112, no. 14, pp. 5263–5266, 2008.

[23] X. Wang, L. J. Zhi, and K. Mullen, "Transparent, conductive graphene electrodes for dye-sensitized solar cells," *Nano Letters*, vol. 8, no. 1, pp. 323–327, 2008.

[24] G. Williams, B. Seger, and P. V. Kamt, "TiO_2-graphene nanocomposites. UV-assisted photocatalytic reduction of graphene oxide," *ACS Nano*, vol. 2, no. 7, pp. 1487–1491, 2008.

[25] I. Jung, D. A. Dikin, R. D. Piner, and R. S. Ruoff, "Tunable electrical conductivity of individual graphene oxide sheets reduced at low temperatures," *Nano Letters*, vol. 8, no. 12, pp. 4283–4287, 2008.

[26] G. Lu, L. E. Ocola, and J. Chen, "Reduced graphene oxide for room-temperature gas sensors," *Nanotechnology*, vol. 20, no. 44, p. 445502, 2009.

[27] W. S. Hummers Jr. and R. E. Offeman, "Preparation of graphitic oxide," *Journal of the American Chemical Society*, vol. 80, no. 6, p. 1339, 1958.

[28] D. R. Dreyer, S. Park, C. W. Bielawski, and R. S. Ruoff, "The chemistry of graphene oxide," *Chemical Society Reviews*, vol. 39, no. 1, pp. 228–240, 2010.

[29] J. T. Robinson, F. K. Perkins, E. S. Snow, Z. Wei, and P. E. Sheehan, "Reduced graphene oxide molecular sensors," *Nano Letters*, vol. 8, no. 10, pp. 3137–3140, 2008.

[30] C. Gómez-Navarro, R. T. Weitz, A. M. Bittner et al., "Electronic transport properties of individual chemically reduced graphene oxide sheets," *Nano Letters*, vol. 7, no. 11, pp. 3499–3503, 2007.

[31] Y. Jin, J. Qian, K. Wang, X. Yang, X. Dong, and B. Qiu, "Fabrication of multifunctional magnetic FePc@Fe3O 4/reduced graphene oxide nanocomposites as biomimetic catalysts for organic peroxide sensing," *Journal of Electroanalytical Chemistry*, vol. 693, pp. 79–85, 2013.

[32] H. Teymourian, A. Salimi, and S. Firoozi, "A high performance electrochemical biosensing platform for glucose detection and IgE aptasensing based on Fe3O4/reduced graphene oxide nanocomposite," *Electroanalysis*, vol. 26, no. 1, pp. 129–138, 2013.

[33] N. T. V. Hoan, N. T. A. Thu, H. V. Duc, N. D. Cuong, D. Q. Khieu, and V. Vo, "Fe3O4/Reduced Graphene Oxide Nanocomposite: Synthesis and Its Application for Toxic Metal Ion Removal," *Journal of Chemistry*, vol. 2016, Article ID 2418172, 2016.

[34] T. Qi, C. Huang, S. Yan, X.-J. Li, and S.-Y. Pan, "Synthesis, characterization and adsorption properties of magnetite/reduced graphene oxide nanocomposites," *Talanta*, vol. 144, pp. 1116–1124, 2015.

[35] L. Guo, P. Ye, J. Wang, F. Fu, and Z. Wu, "Three-dimensional Fe_3O_4-graphene macroscopic composites for arsenic and arsenate removal," *Journal of Hazardous Materials*, vol. 298, pp. 28–35, 2015.

[36] P. S. Teo, H. N. Lim, N. M. Huang, C. H. Chia, and I. Harrison, "Room temperature *in situ* chemical synthesis of Fe_3O_4/graphene," *Ceramics International*, vol. 38, no. 8, pp. 6411–6416, 2012.

[37] M. Zhang and M. Jia, "High rate capability and long cycle stability Fe_3O_4-graphene nanocomposite as anode material for lithium ion batteries," *Journal of Alloys and Compounds*, vol. 551, pp. 53–60, 2013.

[38] A. Prakash, S. Chandra, and D. Bahadur, "Structural, magnetic, and textural properties of iron oxide-reduced graphene oxide hybrids and their use for the electrochemical detection of chromium," *Carbon*, vol. 50, no. 11, pp. 4209–4219, 2012.

[39] X. Y. Yang, X. Y. Zhang, Y. F. Ma, Y. Huang, Y. S. Wang, and Y. S. Chen, "Superparamagnetic graphene oxide–Fe_3O_4 nanoparticles hybrid for controlled targeted drug carriers ," *Journal of Materials Chemistry*, vol. 19, no. 18, pp. 2710–2714, 2009.

[40] Y. Yao, S. Miao, S. Liu, L. P. Ma, H. Sun, and S. Wang, "Synthesis, characterization, and adsorption properties of magnetic Fe_3O_4@graphene nanocomposite," *Chemical Engineering Journal*, vol. 184, pp. 326–332, 2012.

[41] S. Stankovich, D. A. Dikin, R. D. Piner et al., "Synthesis of graphene-based nanosheets via chemical reduction of exfoliated graphite oxide," *Carbon*, vol. 45, no. 7, pp. 1558–1565, 2007.

[42] W. Chen, L. Yan, and P. R. Bangal, "Preparation of graphene by the rapid and mild thermal reduction of graphene oxide induced by microwaves," *Carbon*, vol. 48, no. 4, pp. 1146–1152, 2010.

[43] Y.-P. Chang, C.-L. Ren, J.-C. Qu, and X.-G. Chen, "Preparation and characterization of Fe_3O_4/graphene nanocomposite and investigation of its adsorption performance for aniline and *p*-chloroaniline," *Applied Surface Science*, vol. 261, pp. 504–509, 2012.

[44] L. Feng, M. Cao, X. Ma, Y. Zhu, and C. Hu, "Superparamagnetic high-surface-area Fe_3O_4 nanoparticles as adsorbents for arsenic removal," *Journal of Hazardous Materials*, vol. 217-218, pp. 439–446, 2012.

[45] Y. Zhang, B. Chen, L. Zhang et al., "Controlled assembly of Fe3O4 magnetic nanoparticles on graphene oxide," *Nanoscale*, vol. 3, no. 4, pp. 1446–1450, 2011.

[46] D. Q. Khieu, D. T. Quang, T. D. Lam, N. H. Phu, J. H. Lee, and J. S. Kim, "Fe-MCM-41 with highly ordered mesoporous structure and high Fe content: synthesis and application in heterogeneous catalytic wet oxidation of phenol," *Journal of Inclusion Phenomena and Macrocyclic Chemistry*, vol. 65, no. 1, pp. 73–81, 2009.

[47] Y. Chen, B. Song, X. Tang, L. Lu, and J. Xue, "One-step synthesis of hollow porous Fe 3O 4 beads-reduced graphene oxide composites with superior battery performance," *Journal of Materials Chemistry*, vol. 22, no. 34, pp. 17656–17662, 2012.

[48] V. Chandra, J. Park, Y. Chun, J. W. Lee, I.-C. Hwang, and K. S. Kim, "Water-dispersible magnetite-reduced graphene oxide composites for arsenic removal," *ACS Nano*, vol. 4, no. 7, pp. 3979–3986, 2010.

[49] Y. Qin, M. Long, B. Tan, and B. Zhou, "RhB Adsorption Performance of Magnetic Adsorbent Fe3O4/RGO Composite and Its Regeneration through A Fenton-like Reaction," *Nano-Micro Letters*, vol. 6, no. 2, pp. 125–135, 2014.

[50] J. A. H. Forrest, J. A. Clements, and L. F. Prescott, "Clinical Pharmacokinetics of Paracetamol," *Clinical Pharmacokinetics*, vol. 7, no. 2, pp. 93–107, 1982.

[51] A. Rochefort and J. D. Wuest, "Interaction of substituted aromatic compounds with graphene," *Langmuir*, vol. 25, no. 1, pp. 210–215, 2009.

[52] J. Soleymani, M. Hasanzadeh, N. Shadjou et al., "A new kinetic-mechanistic approach to elucidate electrooxidation of doxorubicin hydrochloride in unprocessed human fluids using magnetic graphene based nanocomposite modified glassy carbon electrode," *Materials Science and Engineering C: Materials for Biological Applications*, vol. 61, pp. 638–650, 2016.

[53] L. Fotouhi, M. Fatollahzadeh, and M. M. Heravi, "Electrochemical behavior and voltammetric determination of sulfaguanidine at a glassy carbon electrode modified with a multi-walled carbon nanotube," *International Journal of Electrochemical Science*, vol. 7, no. 5, pp. 3919–3928, 2012.

[54] E. Laviron, "General expression of the linear potential sweep voltammogram in the case of diffusionless electrochemical systems," *Journal of Electroanalytical Chemistry*, vol. 101, no. 1, pp. 19–28, 1979.

[55] R. Sandulescu, S. Mirel, and R. Oprean, "The development of spectrophotometric and electroanalytical methods for ascorbic acid and acetaminophen and their applications in the analysis of effervescent dosage forms," *Journal of Pharmaceutical and Biomedical Analysis*, vol. 23, no. 1, pp. 77–87, 2000.

[56] P. Masawat, S. Liawruangrath, Y. Vaneesorn, and B. Liawruangrath, "Design and fabrication of a low-cost flow-through cell for the determination of acetaminophen in pharmaceutical formulations by flow injection cyclic voltammetry," *Talanta*, vol. 58, no. 6, pp. 1221–1234, 2002.

[57] R. N. Goyal, V. K. Gupta, M. Oyama, and N. Bachheti, "Differential pulse voltammetric determination of atenolol in pharmaceutical formulations and urine using nanogold modified indium tin oxide electrode," *Electrochemistry Communications*, vol. 8, no. 1, pp. 65–70, 2006.

[58] M. Sharp, M. Petersson, and K. Edström, "Preliminary determinations of electron transfer kinetics involving ferrocene covalently attached to a platinum surface," *Journal of Electroanalytical Chemistry*, vol. 95, no. 1, pp. 123–130, 1979.

[59] A. J. Bard and L. R. Faulkner, *Electrochemical Methods: Fundamentals And Applications*, John Wiley and Sons, New York, NY, USA, 2nd edition, 2001.

[60] W. Horwitz and R. Albert, "The concept of uncertainty as applied to chemical measurements," *Analyst*, vol. 122, no. 6, pp. 615–617, 1997.

[61] B. Saraswathyamma, I. Grzybowska, C. Orlewska et al., "Electroactive dipyrromethene-Cu(II) monolayers deposited onto gold electrodes for voltammetric determination of paracetamol," *Electroanalysis*, vol. 20, no. 21, pp. 2317–2323, 2008.

[62] D. Harvey, *McGraw-Hill Higher Education*, 2000, p. 709.